J Appl Electrochem (2012) 42:257–262
DOI 10.1007/s10800-012-0392-6

ORIGINAL PAPER

Direct electrochemical reduction of Dy_2O_3 in $CaCl_2$ melt

Pyonghun Kim · Hongwei Xie · Yuchun Zhai · Xiangyu Zou · Xiaochuan Lang

Received: 24 October 2011 / Accepted: 6 February 2012 / Published online: 19 February 2012

Abstract The electrochemical reduction of Dy_2O_3 in $CaCl_2$ melt was studied. The cyclic voltammetry, chronoamperometry, AC impedance and constant voltage electrolysis were employed. A single cathodic current peak in the cyclic voltammogram and one response semicircle in the AC impedance spectrum were observed, supporting a one-step electrochemical reduction mechanism of Dy_2O_3. No intermediates were observed by XRD, which confirmed the following electrochemical reduction sequence: $Dy_2O_3 \rightarrow Dy$. The charge transfer resistances and the activation energies involved in the electrochemical reduction step of Dy_2O_3 were obtained by simulating the AC impedance spectra with equivalent circuits. The electrochemical reduction reaction of Dy_2O_3 is controlled by the charge transfer process at a low voltage range and by the diffusion process at a high voltage range.

Keywords Electrochemical reduction · Dy_2O_3 · Molten salt · Metals and alloys · Metallurgy

1 Introduction

The metal dysprosium has good magnetic, optical, electrical and physical properties, and it has thus attracted increasing interest for potential use as various high-tech functional materials. For example, dysprosium is used as an addition agent in the rare earth permanent magnet, magnetostrictive material, magneto-optical material and magnetic refrigeration material. Dysprosium is produced mainly by the calcium thermal reduction of DyF_3, master alloy distillation of DyMg, reduction distillation of Dy_2O_3, and electrochemical reduction of Dy from $DyCl_3$ in molten salts [1–3].

A new method, the cathodic electrochemical reduction of oxides, which is also called the FFC Cambridge process, was used for the preparation of the metal titanium [4]. In the process, titanium dioxide is used as the cathode. On applying a constant voltage between the oxide cathode and carbon anode, oxygen in the cathode is electrochemically ionized, dissolved in the molten salts, and moved to the anode by diffusion, leaving behind pure titanium at the cathode. Titanium, silicon, niobium, chromium, zirconium and tantalum were also prepared by the same method [5–10].

The production of alloys was also studied using electrochemical reduction by treating several oxide mixtures as the cathode and the molten $CaCl_2$ as the electrolyte [11–14]. The electrochemistry of the electrochemical reduction of Nb_2O_5 in eutectic $CaCl_2$–NaCl molten salt has examined by cyclic voltammetry, chronoamperometry and constant voltage electrolysis [15]. The electrochemical reduction mechanism of TiO_2 in $CaCl_2$ molten salt has also been studied by cyclic voltammetry, chronoamperometry and constant voltage electrolysis, and these studies have identified a several—step electrochemical reduction mechanism of TiO_2 [16–18].

There has been no report on the electrochemical reduction of Dy_2O_3 in $CaCl_2$ melt. Hence, the direct electrochemical reduction process of Dy_2O_3 in $CaCl_2$ melt was studied by electrochemical methods.

P. Kim (✉) · H. Xie · Y. Zhai · X. Zou · X. Lang
School of Materials Science and Metallurgy,
Northeastern University, Shenyang 110819,
People's Republic of China
e-mail: jinbingxun@gmail.com

P. Kim
School of Materials Science,
Kim Cheak University of Technology,
Pyongyang, Democratic People's Republic of Korea

2 Experimental

2.1 Electrochemical experiment

Dy_2O_3 (>99.9%) powder was purchased from Sinopharm Chemical Reagent Co. Ltd. Anhydrous $CaCl_2$ (AR) was supplied by Tianjin Kermel Chemical Reagent Co. Ltd. The anode was made of highly pure graphite (99.9%) and was from Sinosteel Shanghai Advanced Graphite Materials Co. Ltd.

High temperature was achieved by a vertical electric resistance furnace equipped with a sealable stainless steel tube reactor, which was connected to a pair of gas lines for the inlet and the outlet of argon. Anhydrous $CaCl_2$ from the analytical reagent was carefully dried in air at 200 °C for 24 h. The metallic cavity electrode (MCE) [19] was fabricated from the Mo rod (3.0 mm diameter, circular through-hole cavity: 1.0 mm diameter, drilled mechanically) and was used as a working electrode to record cyclic voltammograms (CVs) and the chronoamperometric curves of the oxide powder in $CaCl_2$ melt. The oxide powder was manually filled into the MCE cavity by finger—pressing the powders repeatedly on both sides of the rod around the through-hole. Any powder left on the surface of the rod was wiped off carefully. A platinum plate (99.9%, 10 mm width and 30 mm length) was used as the pseudo-reference electrode. The counter electrode was a graphite rod (13 mm diameter and 70 mm total length). Before the experiment, pre-electrolysis was performed to further purify the melt by applying a voltage of −2.0 V between the platinum plate cathode and the graphite rod anode for 6–8 h. Electrochemical measurements were performed on AUTOLAB PGSTAT302 N (Netherlands). AC impedance spectra were measured using a sinusoidal AC signal, and a cathodic potential was applied on the working electrode Dy_2O_3. The amplitude of the AC signal was 5 mV, and the frequency range was between 10^{-2} and 10^4 Hz. The potential overlap covered the potential range of the electrochemical reduction of Dy_2O_3 from −0.5 to −1.8 V.

2.2 Electrolysis experiment

Dy_2O_3 powders were weighed and pressed (20 MPa) into a pellet of 15 mm in diameter with thickness ranging between 1.5 and 2.0 mm. The pellets were sintered in air at 1,300 °C for 6 h. The morphology and the phase composition of the sintered pellets were characterized by SEM (SHIMAZDU SSA-550, Japan) and XRD (X'Pert PRO, Netherlands). After pre-electrolysis, the electrolysis between the oxide pellets (cathode) and the graphite rod (anode) was carried out at a constant voltage ranging between −2.8 and –3.0 V for time duration between 2.5 and 50 h. The experiment was controlled by a DC power source linked to a computer. After electrolysis, the cathode was lifted from the melt and cooled by a stream of argon before its removal from the steel reactor. It was immediately washed in water and alcohol and then dried in a vacuumed desiccator at room temperature for 10 h or longer. The morphology and the phase composition of the products were analyzed by XRD and SEM.

3 Results and discussion

3.1 Cyclic voltammetry and chronoamperometry

Figure 1 shows the cyclic voltammograms with and without Dy_2O_3 in $CaCl_2$ melt at a potential scan rate of 10 mV s^{-1}.

As shown in Fig. 1a, only one cathodic peak corresponding to Dy^{3+} reduction was observed between −1.4 and −1.6 V. Figure 1b shows no peak within the same voltage range. This behavior suggests that the electrochemical reduction of Dy_2O_3 to metal Dy is a one-step reaction. On the way back of the cathodic scan, there is an anodic wave −1.25 V, which appears in both CVs with and without Dy_2O_3. It might be the stripping of Ca metal on the electrode surface. The increase of peak size might be due to the co-deposition of Dy.

Chronoamperometry (Fig. 2) was recorded on the oxide powder by applying a potential between −1.3 and −1.6 V.

As shown in Fig. 2, the current decreases quickly at an early stage and then declines steadily to the background level. However, the currents are smaller with decreasing voltages, thereby suggesting that the faster reduction speed can be attributed to a higher applied voltage. From the data presented later in 3.2, the electrode oxidation is still

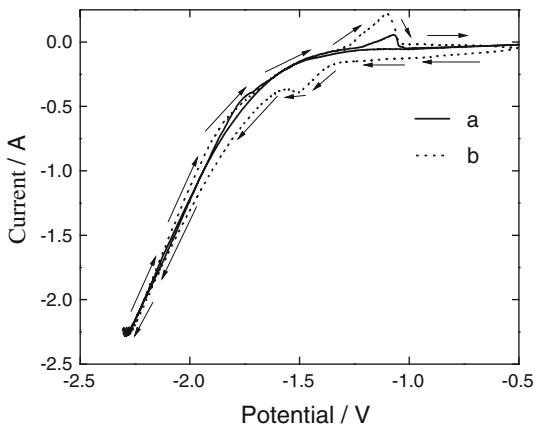

Fig. 1 Cyclic voltammogram of Dy_2O_3 in $CaCl_2$ melt at 900 °C and a potential scan rate of 10 mV s^{-1}: **a** without Dy_2O_3 and **b** with Dy_2O_3

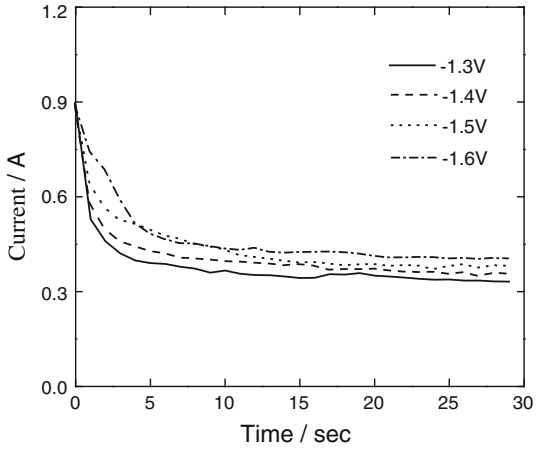

Fig. 2 Chronoamperometry curves of Dy_2O_3 in $CaCl_2$ melt at 900 °C

undergoing after 30 s. The amplitude of these tailing current is proportional to the rate of O species diffuse out from Dy_2O_3 lattice. The higher applied voltage, the faster diffusion, and thus, the bigger current.

3.2 Calculation of the activation energy

In the AC impedance technique, a small sinusoidal potential is applied, and the current response is recorded to provide information about structure, properties, and reaction kinetics. Figure 3 shows the AC impedance spectra of the electrochemical reduction of Dy_2O_3 at different temperatures and voltages.

An AC impedance spectrum consists of a response semicircle. The response semicircle represents a charge transfer step. The AC impedance spectra are roughly semicircular at 800 °C but become semicircular at elevated temperatures, indicating that an increase in temperature speeds up the electrochemical reduction reaction. No change is observed in the number of the response semicircles in the AC impedance spectra with increasing cathodic voltage from −1.4 to −1.6 V and increasing temperature from 800 to 900 °C, further confirming the one-step electrochemical reduction mechanism of Dy_2O_3. Equivalent circuits were used to simulate the AC impedance spectra. In the equivalent circuits, R_s is the resistance of electrolyte $CaCl_2$, R_1 is the charge transfer resistance of the electrochemical reduction step, and CPE_1 is the constant phase element, representing the interfacial capacitances between Dy_2O_3 and the electrolyte. CPE is considered to be a good element to describe the capacitive characteristic of a practical electrode with different degrees of surface roughness, physical nonuniformity, and energetic inhomogeneities. Figure 4 shows the dependency of the charge transfer resistance of the electrochemical reduction step of Dy_2O_3 on the voltage.

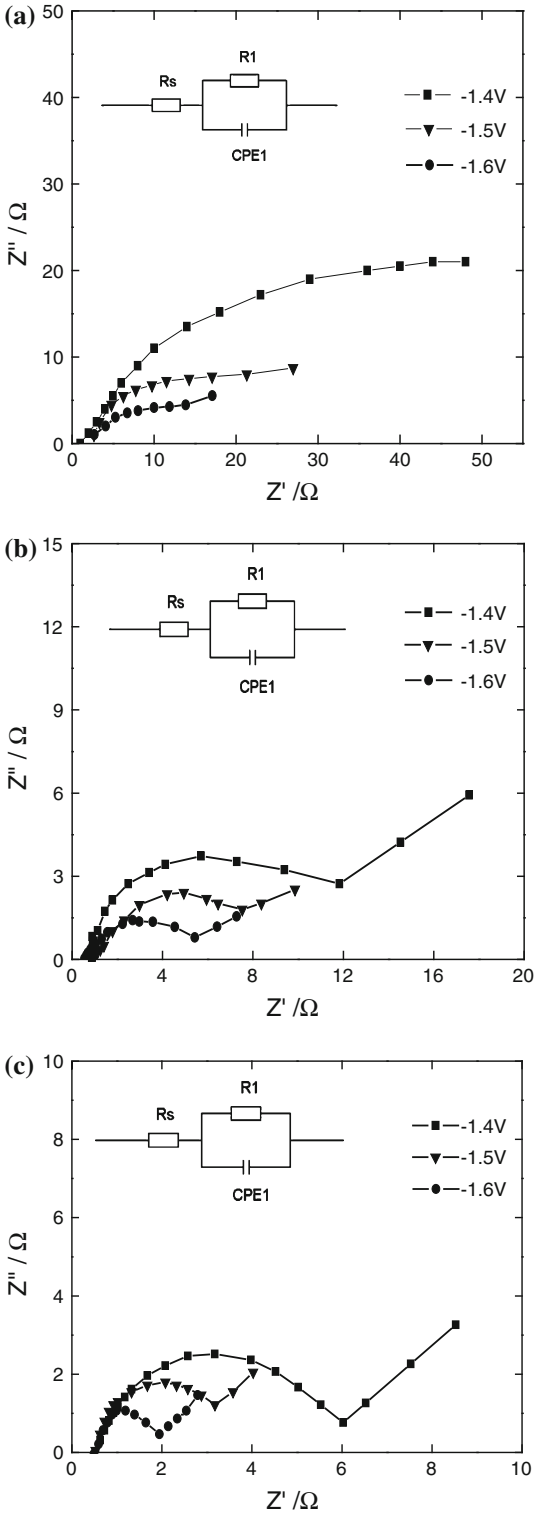

Fig. 3 Dependence of AC impedance spectra on temperature and voltage of Dy_2O_3 in $CaCl_2$ melt: **a** 800 °C, **b** 850 °C, and **c** 900 °C

Charge transfer resistance decreases with increasing cathodic voltage at a low voltage range but remains constant at a high voltage range. This result indicates that the electrochemical reduction reaction is controlled by the

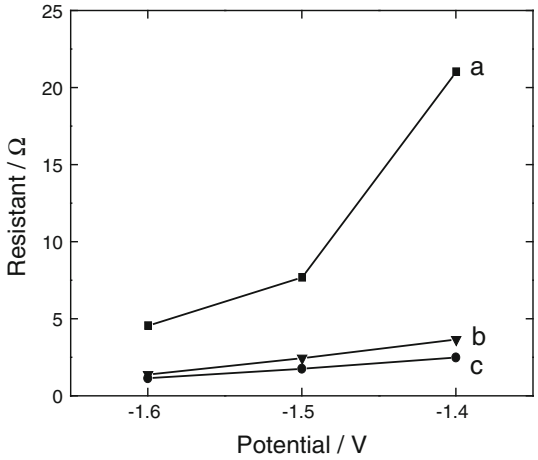

Fig. 4 Dependence of the charge transfer resistance on voltage: **a** 800 °C, **b** 850 °C, and **c** 900 °C

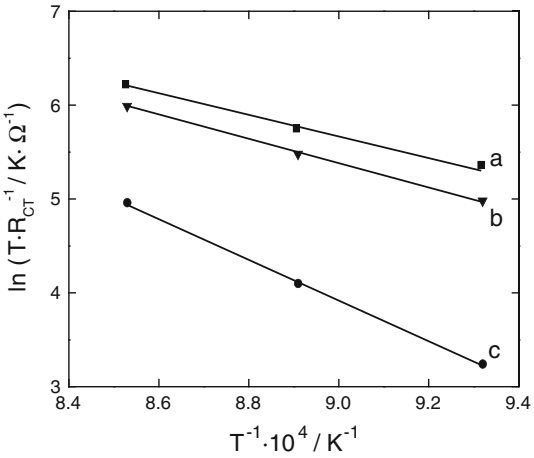

Fig. 5 Dependence of $\ln(T/R_{ct})$ on $1/T$: **a** −1.6 V, **b** −1.5 V, and **c** −1.4 V

charge transfer process at a low voltage range and that it is controlled by diffusion process at a high voltage range.

Charge transfer resistance (R_{ct}) can be expressed by Butler–Volmer equation [20]:

$$R_{ct} = RT/FI_0 \quad (1)$$

where R, F and I_0 are the gas constant, Faraday constant and the current of the charge transfer reaction, respectively. I_0 can be expressed as the following:

$$I_0 = FAkc^{\alpha} \quad (2)$$

A, k, c, and α denote the electrode area, the reaction rate constant, the concentration and the diffusion coefficient of the reactant, respectively. The rate constant is dependent on the temperature by the Arrhenius equation:

$$k = A_0 \exp(-E_a/RT) \quad (3)$$

A_0 is the exponential front factorial, and E_a is the activation energy. Therefore, R_{ct} can finally be expressed as:

$$R_{ct} = RT/\left[F^2 A A_0 \exp(-E_a/RT)\, c^{\alpha}\right] \quad (4)$$

$$R_{ct} = BT/\exp(-E_a/RT) \quad (5)$$

$$\ln(T/R_{ct}) = -E_a/(RT) + C \quad (6)$$

C in Eq. 6 is an arbitrary constant. The straight line slopes between T/R_{ct} and $1/T$ for the electrochemical reduction step of Dy_2O_3 are shown in Fig. 5.

The activation energies of the charge transfer reaction were calculated from the slopes of the lines in Fig. 5 and were between 80 and 200 kJ mol^{-1}.

3.3 Constant voltage electrolysis

To confirm the influence of the electrolysis voltage on the reduction process, different electrolysis voltages (−2.6, −2.8, and −3.0 V) were applied between the oxide pellets cathode and graphite rod anode. The results are shown in Fig. 6.

As shown in Fig. 6a, the current decreases quickly from 1.95 to 0.95 A within 60 min. The current rises subsequently to a broader peak of 1.01 A at 90 min and then declines steadily to the background level of 0.45 A for the remaining electrolysis period. Very similar features can be seen in Fig. 6b and c, where the currents are smaller and the rise of a peak current takes a longer time, thereby reflecting a faster reduction speed that can be attributed to the higher applied voltage. However, if the applied voltage is higher than -3.0 V, it can result in the decomposition of the molten salt. Hence, the optimized electrolysis voltage was considered to be −3.0 V.

To further study the influence of the temperature on the reduction process, experiments were conducted at different temperatures (800, 850, and 900 °C). The results of the experiments are shown in Fig. 7.

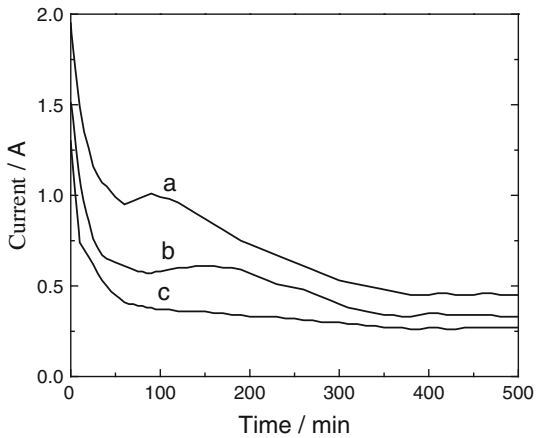

Fig. 6 *I–t* plots of constant voltage electrolysis of Dy_2O_3 at different voltages in $CaCl_2$ melt at 900 °C: **a** −3.0 V, **b** −2.8 V, and **c** −2.6 V

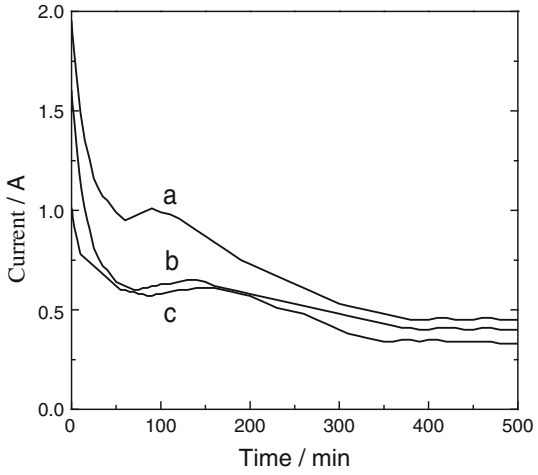

Fig. 7 *I–t* plots of constant voltage electrolysis of Dy_2O_3 at different temperatures in $CaCl_2$ melt at 3.0 V: **a** 900 °C, **b** 850 °C, and **c** 800 °C

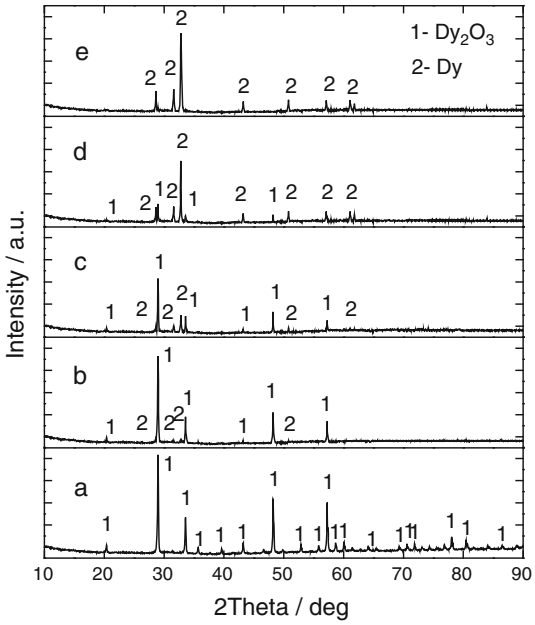

Fig. 8 XRD spectra of the samples before and after electrolysis in $CaCl_2$ melt at 900 °C and −3.0 V: **a** before, **b** 2.5 h, **c** 5 h, **d** 20 h, and **e** 50 h

Similar to the voltage effect, a faster reduction speed of the current can be attributed to a higher applied temperature, although the effects are different in Fig. 7. The decomposition voltage of the molten salt is lower at a higher temperature; hence, higher temperatures have no effect on the deoxidation of the oxide. Therefore, the appropriate temperature was considered to be 900 °C.

The formation of current peaks on the *I–t* plots of electrolysis are generally in agreement with the reduction of the oxide pellets occurring at the metal|oxide|electrolyte three-phase interline (3PI) that expands with time from the initial metal wire-oxide contact point on the pellet's surface (current increases) to the interior of the pellet (current decreases mostly because of difficulties in mass transfer) [19, 21]. The appearance of current peaks in the *I–t* plots of Figs. 6 and 7 may be explained by the reduction of Dy_2O_3 to Dy. The peak represents the expansion of 3PI: Dy|Dy_2O_3|electrolyte in the electro-reduction process.

To further understand the reduction process, electrolysis was performed at −3.0 V for different time durations, and the samples were washed following the same procedure as described above and then analyzed by XRD. The XRD spectra are shown in Fig. 8.

As shown in Fig. 8, when the current reached the trough after 2.5 h of electrolysis, the washed product was primarily dominated by Dy_2O_3. After 5 h of electrolysis, both Dy_2O_3 and Dy were detectable. However, after 20 h of electrolysis, Dy was detected but relatively little Dy_2O_3 was revealed by the spectrum. The 50 h electrolysis sample was dominated by Dy. These results agree very well with the explanation given before for the existence of a single peak in Figs. 6 and 7. On the basis of these results, the reduction process can be speculated as follows:

$$Dy_2O_3 + 6e^- \rightarrow 2Dy + 3O^{2-} \quad (7)$$

The SEM images of the sintered oxide pellets and the reduced products at 900 °C and −3.0 V for 50 h are shown in Fig. 9.

It can be concluded from Figs. 8 and 9 that the practical electrolysis voltage for the formation of pure metallic dysprosium from solid Dy_2O_3 in a molten salt is approximately −3.0 V at 900 °C, although the theoretical decomposition voltage is approximately −2.62 V at 900 °C by thermodynamic calculation.

4 Conclusions

Cyclic voltammetry, chronoamperometry and AC impedance are good techniques to characterize the electrochemical reduction reaction of Dy_2O_3 in $CaCl_2$ melt. The electrochemical reduction reaction of Dy_2O_3 in $CaCl_2$ melt follows the mechanism $Dy_2O_3 \rightarrow Dy$. The results of the electrochemistry experiments represent the expansion of 3PIs:Dy|Dy_2O_3|electrolyte in the electro-reduction process. The electrochemical reduction reaction is controlled by the charge transfer process at a low voltage range and by diffusion process at a high voltage range. The activation energy of the electrochemical reduction step is between 80 and 200 kJ mol^{-1}. The optimized electrolysis voltage and temperature of Dy_2O_3 in $CaCl_2$ melt were found to be −3.0 V and 900 °C, respectively.

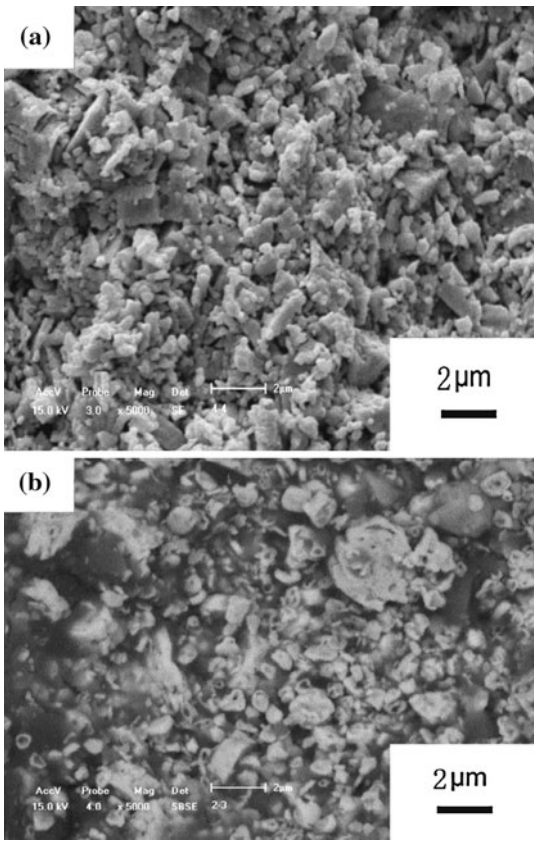

Fig. 9 SEM images of the samples **a** before electrolysis and **b** after electrolysis in $CaCl_2$ melt at 900 °C and −3.0 V for 50 h

Acknowledgment The authors acknowledge gratefully the financial support from "The Fundamental Research Funds for Central University in China" (Grant No. N100302008).

References

1. Lin HC (2001) Production, application and market status of rare earths chloride in home. Chin Rare Earths 22:75
2. Zhang SR (2000) Manufacture, refining and application of dysprosium metal. Rare Metals Cem Carbides 142:53
3. Castrillejo Y, Bermejo MR, Barrado AI, Pardo R, Barrado E, Mart′ınez AM (2005) Electrochemical behaviour of dysprosium in the eutetic LiCl-KCl at W and Al electrode. Electrochim Acta 50:2047
4. Chen GZ, Fray DJ, Farthing TW (2001) Direct electrochemical reduction of titanium dioxide to titanium in molten calcium chloride. Nature 407:361
5. Fray DJ, Chen GZ (2005) Reduction of titanium and other metal oxides using electrodeoxidation. Mater Sci Tech 20:295
6. Jin XB, Gao P, Wang DH, Hu XH, Chen GZ (2003) Electrochemical preparation of silicon and its alloys from solid oxides in molten calcium chloride. Angew Chem Int Ed 43:733
7. Gordo E, Chen GZ, Fray DJ (2004) Toward optimisation of electrolytic reduction of solid chromium oxide to chromium powder in molten chloride salts. Electrochim Acta 49:2195
8. Yan XY, Fray DJ (2002) Production niobium powder by direct electrochemical reduction of solid Nb_2O_5 in a eutetic $CaCl_2$–NaCl melt. Metall Mater Trans B 33:685
9. Suddhasattwa G, Vandarkuzhali S, Venkatesh P, Seenivasan G, Subramanian T, PrabhakaraReddy B, Nagarajan K (2009) Electrochemical studies on the redox behaviour of zirconium in molten LiCl–KCl eutectic. J Electroanal Chem 627:15
10. Song QS, Xu Q, Kang X, Du JH, Xi ZP (2010) Mechanistic insight of electrochemical reduction of Ta_2O_5 to tantalum in a eutectic CaCl–NaCl molten salt. J Alloy Compd 490:241
11. Muir Wood AJ, Copcutt CR, Chen GZ, Fray DJ (2003) Electrochemical fabrication of nickel manganese gallium alloy powder. Adv Eng Mater 5:650
12. Fenn AJ, Cooley G, Fray DJ, Smith L (2004) Exploting the FFC Cambridge process. Adv Mater Process 162:51
13. Glowacki BA, Fray DJ, Yan XY (2003) Superconducting Nb_3Sn intermetallics made by electrochemical reduction of Nb_2O_5–SnO_2 oxides. Physica 387:242
14. Qiu GH, Wang DH, Ma M, Jin XB, Chen GZ (2006) Electrolytic synthesis of $TbFe_2$ from Tb_4O_7 and Fe_2O_3 powder in molten $CaCl_2$. J Electroanal Chem 589:139
15. Wang SL, Xue Y, Sun H (2006) Electrochemical study on the electrodeoxidation of Nb_2O_5 in equimolar $CaCl_2$ and NaCl melt. J Electroanal Chem 595:109
16. Wang SL, Li YJ (2004) Reaction mechanism of direct electroreduction of titanium dioxide in molten calcium chloride. J Electroanal Chem 571:31
17. Schwandt C, Fray DJ (2005) Determination of the kinetic pathway in the electrochemical reduction of titanium dioxide in molten calcium chloride. Electrochim Acta 51:66
18. Dring K, Dashwood R, Inman D (2005) Voltammetry of titanium dioxide in molten calcium chloride at 900 °C. J Electrochem Soc 152:E104
19. Chen GZ, Gordo E, Fray DJ (2004) Direct electrolytic preparation of chromium powder. Metall Mater Trans B 35:223
20. Wang SZ, Jiang Y, Zhang YH (1998) AC impedance study of the La0.8Sr0.2MnO3/YSZ electrode. Electrochemistry 4:252
21. Chen GZ, Fray DJ (2001) In: Chen NY, Qiao ZY (eds) Proceedings of the 6th international symposium on molten salt chemical technology. Shanghai University Press, Shanghai, p 79